Journal of Materials Chemistry A

Accepted Manuscript

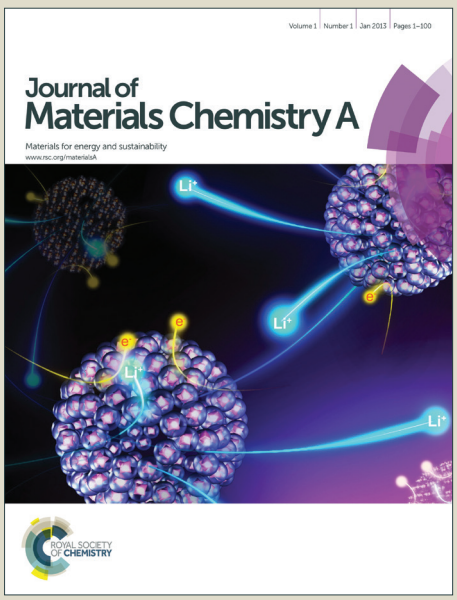

ROYAL SOCIETY OF CHEMISTRY

www.rsc.org/materialsA

Journal of Materials Chemistry A

Dynamic Article Links ►

Cite this: DOI: 10.1039/c0xx00000x

www.rsc.org/xxxxxx

ARTICLE TYPE

Sulfur doped Graphitic Carbon Nitride Decorated with Graphene Quantum Dots for Efficient Metal-free Electrocatalyst

Chenyu Xu,‡ Qing Han,‡ Yang Zhao,* Lixia Wang, Yang Li, and Liangti Qu*

Received (in XXX, XXX) Xth XXXXXXXXX 20XX, Accepted Xth XXXXXXXXX 20XX

DOI: 10.1039/b000000x

A rationally designed strategy has been developed for spontaneous reduction and assembly of graphene quantum dots rich with carbonyl and carboxylic groups (ox-GQDs) onto sulfur doped graphitic carbon nitride (s-g-C_3N_4) nanosheets to form unique s-g-C_3N_4@GQDs nanohybrids by a one-step hydrothermal treatment. The fabricated architectures exhibit remarkably enhanced catalytic activity in oxygen reduction reaction far better than the original s-g-C_3N_4 and GQDs, which is even comparable to those well-developed graphene and GQDs-based catalysts, demonstrating the potential towards energy conversion applications.

Introduction

The oxygen reduction reaction (ORR) is an important process for the electrochemical energy conversion devices that directly convert chemical energy to electric power. Noble metal catalyst, such as platinum, is the most efficient ORR catalysts used in fuel cell cathodes.[1,2] However, it suffers from its high price and weak durability.[3,4] The development of high-performance and low-cost catalytic materials for the ORR has been a major challenge for the large-scale application of fuel cells.[5–7] Although Pt alloys or other non-noble metals based materials have been developed as substitute catalysts for the ORR,[8–11] they still suffer from multiple disadvantages, such as vulnerability to fuel crossover, and harmfulness to the environment.[9] Thus, the continuous search for non-metal catalysts with high activity for the ORR has attracted much attention.

Graphitic carbon nitride (g-C_3N_4) with a prototypical two-dimensional (2D) graphitic structure, has received increasing attention among the carbon nitride family due to its interesting electronic properties, promising catalytic activities, high in-plane nitrogen content and environmental friendly feature, which has been explored in the field of photocatalysis, bioimaging, CO_2 reduction and other energy conversion process.[12–17] Recently, g-C_3N_4 doped with heteroatom (such as sulfur, boron, iodine etc.) has been demonstrated to be effective to narrow down band gap and enhance its catalytic activities.[18–21] In spite of this, g-C_3N_4 and its derivatives are still restricted in the electrochemical-related applications due to the inherent low electronic conductivity and low surface area.

Graphene quantum dots (GQDs), single or few-layer graphenes with a tiny size of only several nanometers, stand for a new type of quantum dots (QDs) and have received extensive interest in materials science and engineering.[22–25] Due to the remarkable quantum-confinement, high exposed surface and edge effects, GQDs possess good electrical conductivity, tunable band gaps and extraordinary optoelectronic properties,[22–27] thus leading to multifunctional applications in photovoltaic devices,[23] pollutant detection,[28] fuel cells[24] and others energy related fields.[29] It was found that functionalized GQDs or GQDs based hybrid composites can present the collective properties of the individual GQDs which have been particularly used as catalysts or supports toward ORR.[24, 30–32] For example, N-doped GQDs or its well-organized architectures displayed excellent performance toward ORR in alkaline solutions.[24,30] Besides, GQDs were also served as the supporting substrates of Pt nanoparticles, showing the enhanced catalytic activity in ORR.[31, 32] However, to the best of our knowledge, the combination of the sulfur doped g-C_3N_4 and GQDs has never been achieved for efficient catalytic performance in ORR.

Herein, we have developed the rationally assembly of zero dimensional (0D) GQDs in-situ decorated onto the 2D sulfur doped graphitic carbon nitride (s-g-C_3N_4) nanosheets to form unique s-g-C_3N_4@GQDs nanohybrids by a simple one-step hydrothermal method. Such unique 2D architecture for s-g-C_3N_4@GQDs can be used as a new class of metal-free electrocatalysts for the ORR and shows remarkably enhanced catalytic activity far better than that of original s-g-C_3N_4 and GQDs, even comparable to those well-developed graphene and GQDs-based catalysts. The s-g-C_3N_4@GQDs demonstrated in this study opens the way for constructing the new type of g-C_3N_4 based nanostructured materials, showing the great potential for energy conversion applications.

Experimental

Synthesis of the s-g-C_3N_4

The s-g-C_3N_4 samples were prepared as follows: Firstly, 10 g melamine powder (Fine Chemical Research Institute, Tianjin, China) was heated at 550 ^oC for 4 h. The yellow bulk g-C_3N_4 was obtained after cooling to room temperature. Then, the obtained g-

C_3N_4 (0.5 g) and sulfur powder (1.5 g, Sinopharm Chemical Reagent Co., Ltd) were mixed together and placed into a stainless steel capsule containing stainless steel balls of 6 mm in diameter. The container was fixed in the planetary ball-mill machine and agitated with 25 Hz for 48 h. Finally, the s-g-C_3N_4 nanosheets were obtained by washing residue with CCl_3, ethanol and deionized water in turn and followed by heating at 300 °C for 1h to remove the excess sulfur.

Synthesis of ox-GQDs

The ox-GQDs was prepared by oxidation of the natural graphite powder (Aladdin) using a modified chemical oxide method as reported in our previous paper.[31] In a typical experiment, Graphite (1.0 g) was added to 100 ml concentrated sulfuric acid (H_2SO_4, Beijing Chemical Works) under stirring at room temperature, followed by adding 43.0 g sodium nitrate ($NaNO_3$, Beijing Chemical Works) and then the mixture was cooled to 0 °C. Under vigorous stirring, 3.0 g potassium permanganate ($KMnO_4$, Beijing Chemical Works) was added slowly with the reaction temperature maintaining below 20 °C. After that, the mixture was then transferred to a 120 °C oil bath and stirred for 12 h. After cooling to room temperature, the obtained mixture was diluted with 500 ml deionized water. Then the sodium carbonate (Na_2CO_3, Beijing Chemical Works) was added in the mixture solution until pH=3. Finally, the ox-GQDs were obtained by dialyze the diluted solution for 3 days.

Synthesis of the s-g-C_3N_4@GQDs nanohybrids

For preparation of the s-g-C_3N_4@GQDs nanohybrids, 3 ml homogeneous ox-GQDs (0.26 mg/ml) and 50 mg s-g-C_3N_4 were sealed in a 10 ml Teflon-lined autoclave and maintained at 230 °C for 3 h. After the autoclave was naturally cooled down to room temperature, the s-g-C_3N_4@GQDs was freeze-dried. In order to enhance the conductivity and connection between s-g-C_3N_4 and GQDs, the samples were then heated at 400 °C for 1 h with a heating speed of 5 °C/min under Ar atmosphere.

Electrochemical measurements

The 2 mg s-g-C_3N_4@GQDs was first ultrasonically dispersed in 0.5 ml ethanol with 50 μl of Nafion solution (5 %). For electrochemical measurement: 6μl of the ink was dipped on a glass carbon electrode (GC, ca. 0.196 cm^2) and dried in air. The mass loading is 0.12 mg/cm^2. 0.1 M PBS solution containing 0.1 M KCl solution was used as electrolyte. The potential range for cyclic voltammograms (CV) test was -0.1–0.5V. The scan rate is 10mV/s.

For ORR measurement: the mixed suspensions (~2.5 μl) were dipped onto GC electrode (ca. 0.25 cm^2) as working electrode with the mass loading of 0.04 mg/cm^2. Measurements on a rotating disk electrode (RDE) and/or rotating ring-disk electrode (RRDE) were carried out on a MSRX electrode rotator (Pine Instrument) and the CHI 760D potentiostat equipped with MSRX electrode rotator (Pine Instrument). 0.1 M KOH was used as the electrolyte. A Pt wire and Ag/AgCl were used as counter and reference electrodes, respectively. The CV curves were recorded by applying a linear potential scan between -0.8 V and 0.2 V at a scan rate of 10 mV/s. RDE measurements were conducted at different rotating speeds from 0 to 2000 rpm. The commercial Pt/C catalyst (20 wt% platinum on carbon black) with the similar amount (~10 μg) was also studied for comparison. N_2 or O_2 was used to give the O_2-free or O_2-saturated electrolyte solution.

The transferred electron number (n) per O_2 molecule was calculated from Koutecky-Levich (K-L) equation.[33a] The current density j is related to the rotation rate ω of the electrode according to

$$1/j = 1/j_k + 1/B\omega^{0.5} \quad (1)$$

where j_k is the kinetic current and B is Levich slope which is given by

$$B = 0.2nF(D_{O2})^{2/3}v^{-1/6}C_{O2} \quad (2)$$

Here n is the number of electrons transferred in the reduction of one O_2 molecule, F is the Faraday constant (F = 96485 C mol^{-1}), D_{O2} is the diffusion coefficient of O_2 in 0.1M KOH (D_{O2} =1.9 $\times 10^{-5}$ cm^2 s^{-1}), v is the kinematics viscosity (v = 0.01 cm^2 s^{-1}) and C_{O2} is concentration of O_2 in the solution (D_{O2} = 1.2 × 10^{-6} mol cm^{-3}).[24, 33b, c] The constant 0.2 is adopted when the rotation speed is expressed in rpm.

The n was also determined from the RRDE measurement.

$$n = 4I_d / (I_d + I_r/N) \quad (3)$$

The peroxide percentage (% HO_2^-) was calculated based on the equation:

$$\%HO_2^- = 200 \times I_r/N/(I_d + I_r/N) \quad (4)$$

Here I_d and I_r is the disk current and ring current, respectively, and N is the current collection efficiency of Pt ring and determined to be 0.37.[24]

Characterization

The morphology was investigated by scanning (SEM, JSM-7500F) and transmission (TEM, 7650B, Hitachi) electron microscopy and the elemental mappings were performed on a scanning transmission electron microscope (STEM) unit with high-angle annular dark-field (HAADF) detector (HITACHI S-5500) operating at 30kV. X-ray diffraction (XRD) patterns were carried out using a Netherlands 1710 diffractometer with a Cu Kα irradiation source (λ = 1.54 Å), and a self-calibration process was performed with a SiO_2 internal standard sample prior to target measurement. Raman spectra were recorded using a RM 2000 Microscopic Confocal Raman Spectrometer (Renishaw PLC, England) with a 514.5 nm laser. X-ray photoelectron spectroscopy (XPS) data were obtained with an ESCALab220i-XL electron spectrometer from VG Scientific using 300W AlKα radiation.

Results and discussion

The GQDs rich with carbonyl and carboxylic groups on the surfaces named as ox-GQDs were produced by chemical oxidation method (Fig. 1a and b). The as-prepared ox-GQDs solution was found to exhibit a homogeneous phase without any noticeable precipitation at room temperature. Under irradiation by a 365 nm lamp, the ox-GQDs emitted intense yellow-brown luminescence due to existence of the carbonyl and carboxylic groups (Figure 1a right). Fig. 1b shows the TEM image of the ox-GQDs which are monodisperse with a fairly uniform diameter of ca. 2–7 nm. For the preparation of the s-g-C_3N_4 nanosheets, the g-C_3N_4 nanosheets were ball-milled with sulfur powder for 48h. The s-g-C_3N_4 nanosheets were obtained after repeated washing and treated at 300 °C for 1h. As demonstrated in Fig. 1c, the as-

prepared s-g-C_3N_4 shows a uniform small sheets which is also further confirmed by the corresponding TEM image (Fig. 1d).

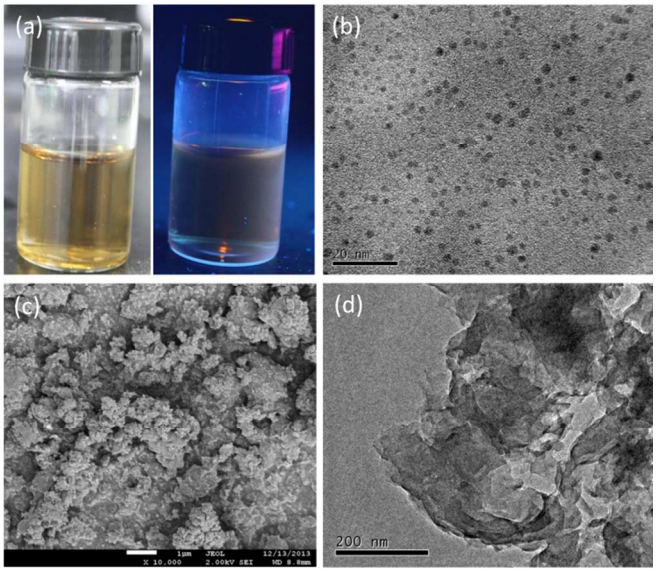

Fig. 1 (a) The photos of ox-GQDs (left) and under the irradiation (right) by a 365 nm lamp (16 W). (b) The TEM image of ox-GQDs. (c, d) The SEM and TEM images of s-g-C_3N_4, respectively. Scale bars: b) 20 nm, c) 1 μm, d) 200 nm.

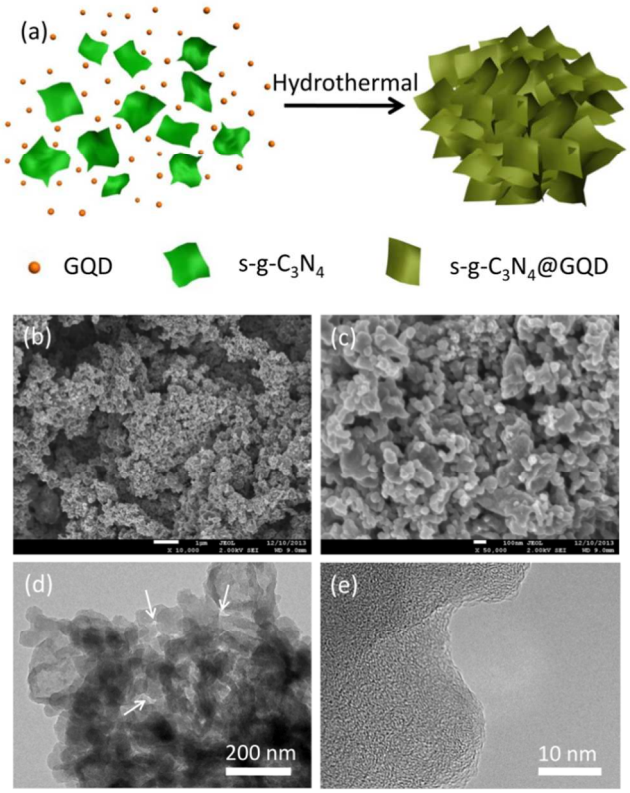

Fig. 2 (a) The fabrication process of s-g-C_3N_4@GQDs. (b, c) The SEM images of s-g-C_3N_4@GQDs. (d) The TEM image of as-prepared s-g-C_3N_4@GQDs, and (e) the corresponding high resolution TEM image of (d). Scale bars: b) 1 μm, c) 100 nm, d) 200 nm, e) 10 nm.

The process for the fabrication of s-g-C_3N_4@GQDs nanohybrids is illustrated in Fig. 2a. To achieve the s-g-C_3N_4@GQDs, the mixture of the s-g-C_3N_4 nanosheets and ox-GQDs were treated by hydrothermal treatment at 230 ^oC for 3 h. In order to enhance the conductivity and connection between s-g-C_3N_4 and GQDs, the samples were then heated at 400 ^oC for 1 h under Ar atmosphere. Due to the π-π interaction, either the separate ox-GQDs or s-g-C_3N_4 nanosheets, exhibits serious aggregated nanospheres or large stacking sheets after hydrothermal treatment (Fig. S1). After combination of ox-GQDs and s-g-C_3N_4, as shown in Fig. 2b and c, the s-g-C_3N_4@GQDs shows a nanojunction structure with nanosheets cross-linking together which is further confirmed by TEM image (Fig. 2d). The TEM image of s-g-C_3N_4@GQDs also reveals the arisen nanopore structure formed by cross-linked sheets (decorated with arrows in Fig. 2d), which would enhance the catalytic activity in the electrochemical behaviors. Although most of the intrinsic lattice structures for both ox-GQDs and s-g-C_3N_4 can't be observed in the prepared s-g-C_3N_4@GQDs, small scattered lattice structures belonging to s-g-C_3N_4 are still recognized in Fig. 2e.

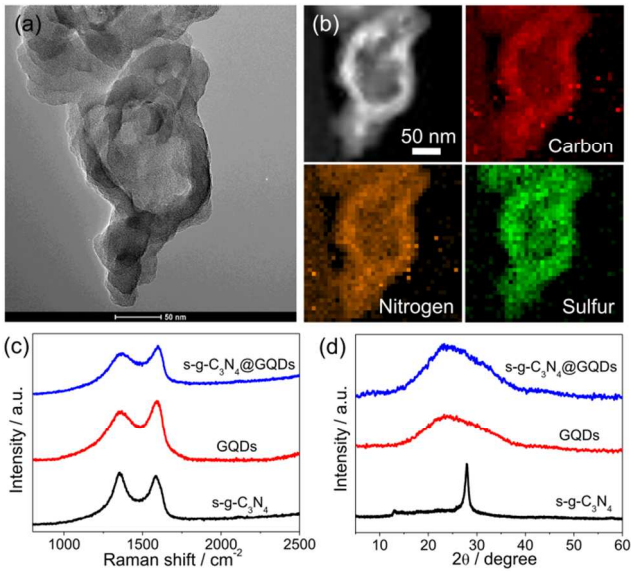

Fig. 3 (a) STEM image of the s-g-C_3N_4@GQDs. (b) The corresponding C-, N- and S- elemental mappings. (c, d) Raman spectra and XRD patterns of s-g-C_3N_4, GQDs and s-g-C_3N_4@GQDs, respectively.

The typical STEM images of s-g-C_3N_4@GQDs are demonstrated in Fig. 3 a and b. In Fig. 3b, the C, N, and S elements are uniform distributed all over the as-prepared s-g-C_3N_4@GQDs basal plane, consistent with the energy-dispersive spectrometry (EDS) (Fig. S2).

As shown in Fig. 3c, Raman spectra of the original s-g-C_3N_4 exhibits two representative bands indexed at ~1350 (D band) and ~1580 cm^{-1} (G band) which can be attributed to disordered sp^2 caused by the linking with N atoms and graphite-like sp^2 microdomains, respectively.[34] While the GQDs obtained by the hydrothermal treatment shows two typical bands centered at around ~1350 and ~1580 cm^{-1} belonging to the well-documented D and G bands of carbon materials.[23,24] Interestingly, all of the Raman spectra of s-g-C_3N_4@GQDs show two characteristic D

and G bands without any other substances signal indicating an efficient and mild combination of s-g-C_3N_4 and GQDs. It was observed that the I_D/I_G ratio (0.96) for s-g-C_3N_4@GQDs was similar with that of GQDs (0.93) and much lower than the original s-g-C_3N_4 (1.07), showing that the appearance of s-g-C_3N_4 did not cause an obvious effect on the crystalline structure of s-g-C_3N_4@GQDs.

The XRD patterns of s-g-C_3N_4@GQDs in comparison with s-g-C_3N_4 and GQDs samples are shown in Fig. 3d. The s-g-C_3N_4 represents the diffraction peak at 27.3° corresponding to the (002) peak of s-g-C_3N_4 attributed to inter-planar stacking peak of conjugated aromatic systems. A weak broad peak at around 13° belongs to the (001) peak of s-g-C_3N_4 which is consistent with an in-plane structural motif between nitride pores.[35,36] Unlike the original s-g-C_3N_4, the GQDs obtained by the hydrothermal treatment exhibits a broad reflection peak at ca. 23.6°, similar with that of the graphene film (ca. 23.5°).[24] After combination of s-g-C_3N_4 and GQDs, the characteristic peaks for s-g-C_3N_4 were almost overlapped by GQDs, leading to a much broader peak for the prepared s-g-C_3N_4@GQDs, indicating that the GQDs are successfully drafted on the surface of s-g-C_3N_4 nanosheets.

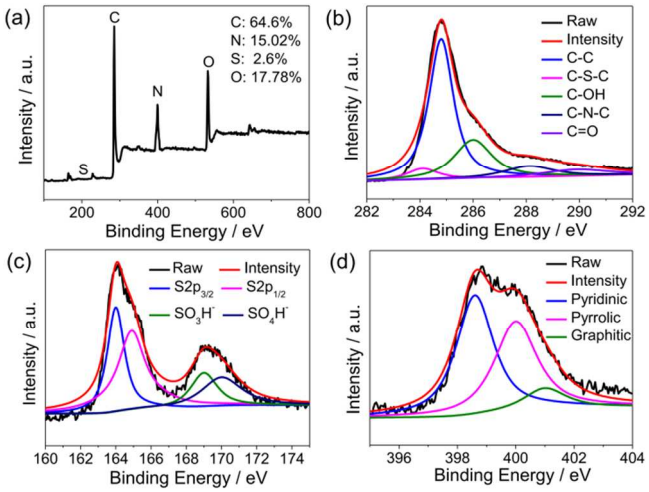

Fig. 4 (a) XPS spectra of s-g-C_3N_4@GQDs and the corresponding high-resolution C 1s (b), S 2p (c) and N 1s (d) peaks, respectively.

The XPS measurement demonstrated in Fig. 4 was also performed to investigate the chemical composition of C, N and S in s-g-C_3N_4@GQDs. As shown in Fig. 4a, the survey spectrum of XPS shows the pronounced peaks for N 1s and S 2p corresponding to an N and S content of 15.02 at% and 2.6 at%, respectively, apart from C and O elements. The high-resolution C 1s spectrum is shown in Fig. 4b. The peak at 284.8 eV belongs to C-C coordination, the peak centered at 288.3 eV corresponds to C-N coordination of s-g-C_3N_4 and the C-S-C peak appears at around 284.0 eV. Fig. 4c shows the high-resolution S 2p spectrum with two peaks at 163.8 and 165.0 eV belonging to the C-S-C structure. The peaks at 169 and 170 eV belong to SO_3H^- and SO_4H^-, indicating that the S elements are partially doped into the g-C_3N_4 sheets.[37] The high-resolution N 1s spectrum (Fig. 4d) reveals the typical nitrogen peaks, including pyridine-like (398.8 eV), pyrrolic (400.5 eV), and graphitic (401.1 eV) N species, which are also confirmed by C-N-C peak in the C 1s spectrum of s-g-C_3N_4@GQDs hybrids (Fig. 4d).

The electrochemical behavior of s-g-C_3N_4@GQDs was investigated in comparison with common GQDs and the original s-g-C_3N_4 in a bio-compatible system of 0.1 M PBS containing 0.1 M KCl (Fig. S3).[38] The CV curve for s-g-C_3N_4@GQDs exhibits a typical capacitive behavior with an overall larger response current than that of GQDs and the original s-g-C_3N_4, indicating the more active sites and efficient charge separation and transfer channel within s-g-C_3N_4@GQDs.[38]

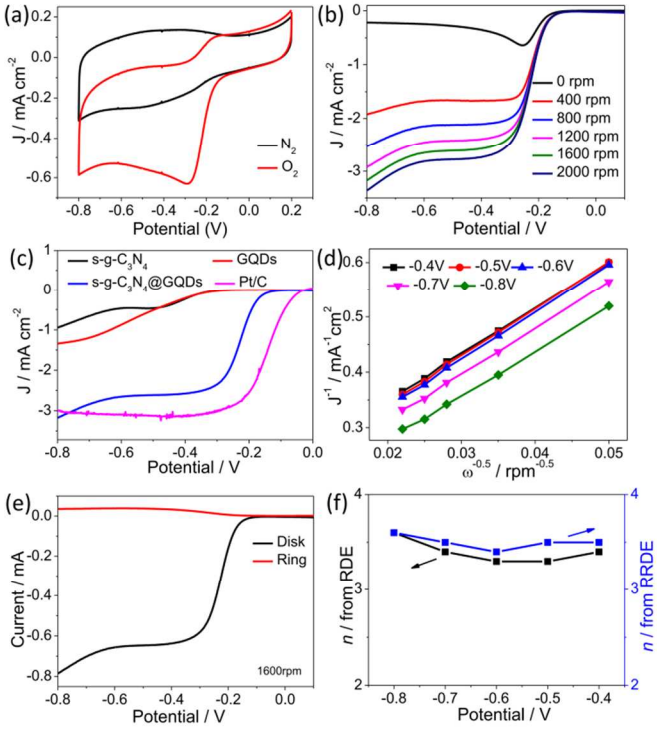

Fig. 5 (a) CV curves of s-g-C_3N_4@GQDs in an O_2- or N_2-saturated 0.1M KOH solution at a scan rate of 10 mV/s. (b) The linear sweep voltammogram (LSV) curves of the s-g-C_3N_4@GQDs in O_2-saturated 0.1 M KOH solution at different rotating speeds. The scan rate is 10 mV/s. (c) LSV of various electrodes on a RDE (1600 rpm) in O_2-saturated 0.1 M KOH solution at a scan rate of 10 mV/s.(d) K-L plots derived from LSV curves at different potentials from -0.4 V to -0.8 V. (e) RRDE curves of the s-g-C_3N_4@GQDs at 1600 rpm. (f) The *n* derived from the K-L equation (Eq. 1 and 2) and RRDE curves (Eq. 3 and 4) with the potential of -0.4 to -0.8 V.

The ORR electrochemical activity for s-g-C_3N_4@GQDs was investigated in an O_2-saturated 0.1M KOH solution with s-g-C_3N_4 and GQDs as compared catalysts. The CV curves of s-g-C_3N_4@GQDs shown in Fig. 5a exhibit an excellent O_2 reduction peak at ca. -0.27 V which is more positive than s-g-C_3N_4 and GQDs (Fig. S4) and compared to those heteroatom doped graphene and GQDs-based materials.[24,30,39] The LSV measured on RDE for s-g-C_3N_4@GQDs at different electrode rotation rates were demonstrated in Fig. 5b. The diffusion current densities of the s-g-C_3N_4@GQDs catalyst increased with increasing rotation speed which is larger than that of compared catalysts (Fig. S5). LSV curves in Fig. 5c for various catalysts including s-g-C_3N_4, GQDs, commercial Pt/C and s-g-C_3N_4@GQDs revealed that the

s-g-C_3N_4@GQDs has an onset potential of ca. -0.07 V closer to the commercial Pt/C at ca. -0.01V and more positive than that of s-g-C_3N_4 (ca. -0.23 V) and GQDs (ca. -0.20 V) catalysts, indicating a facile ORR process for s-g-C_3N_4@GQDs. Besides, the ORR diffusion current density of the s-g-C_3N_4@GQDs is significant higher than those of other catalysts, and even reach to that of the Pt/C electrode at a potential at -0.8 V, indicating the high electrochemical activity. [40]

The K-L plots for s-g-C_3N_4@GQDs electrode obtained from the LSV curves with the potential of -0.4 to -0.8 V shows a good linear relationship (Fig. 5 b and d). After calculating from the slope of the K-L plots, the *n* is determined to be approximately 3.5 based on the K-L equation (Eq. 1 and 2) indicating a nearly four electron pathway for the ORR process which is also confirmed by the RRDE measurements (Fig. 5e). As shown in Fig. 5 e and f, the *n* obtained from the RRDE curves (Eq. 3 and 4) is similar to that calculated from the RDE curves (Eq. 1 and 2).

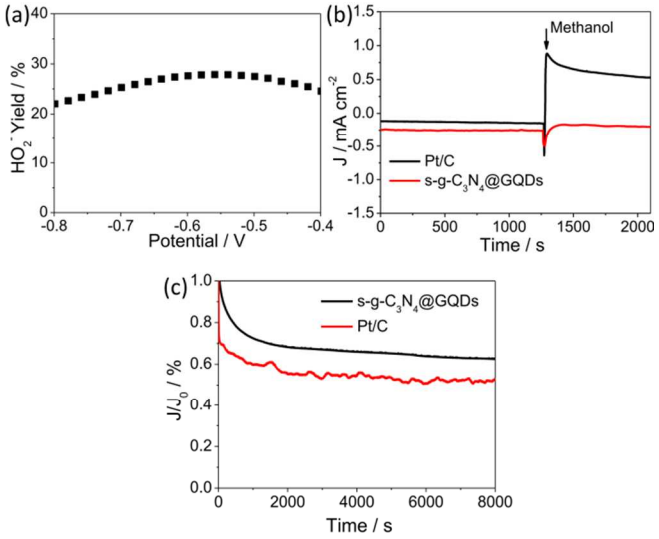

Fig. 6 (a) HO_2^- yield on the s-g-C_3N_4@GQDs electrode. (b) Crossover toleration test of the s-g-C_3N_4@GQDs and Pt/C at -0.30 V in an O_2-saturated 0.1 M KOH solution. The arrow shows the addition of 10 vol% methanol into the O_2-saturated electrochemical cell. (c) Electrochemical durability test of s-g-C_3N_4@GQDs and Pt/C at -0.3 V (1600 rpm) in an O_2-saturated 0.1 M KOH solution.

The corresponding HO_2^- yield on the s-g-C_3N_4@GQDs electrode during the ORR process was also investigated in Fig. 6a, which was below 30 % over the entire potential range from -0.4 to -0.8 V, indicating the efficient reduction of O_2 to OH^- for s-g-C_3N_4@GQDs. Fig. 6b demonstrated the methanol crossover effect for s-g-C_3N_4@GQDs and commercial Pt/C catalysts. The prepared s-g-C_3N_4@GQDs exhibit no obvious change of current density after adding methanol (10 vol%) into the electrolyte, whereas a sharp anodic current owing to the methanol oxidation reaction was observed for the commercial Pt/C catalyst, indicating a remarkable crossover tolerance for s-g-C_3N_4@GQDs to the fuel molecule methanol. Furthermore, the durability of s-g-C_3N_4@GQDs in comparison with Pt/C catalyst was also investigated by chronoamperometric measurements at -0.3 V in O_2-saturated 0.1 M KOH solution (Fig. 6c). Although the s-g-C_3N_4@GQDs shows a much large decrease in its activity during 8000 s testing period, it is still superior to that of Pt/C, suggesting a good stability of s-g-C_3N_4@GQDs in alkaline media.

Conclusions

In this work, we have developed a rationally designed strategy for spontaneous reduction and assembly of ox-GQDs onto s-g-C_3N_4 nanosheets to form unique s-g-C_3N_4@GQDs nanohybrids by a one-step hydrothermal treatment. As a new metal-free catalyst, the prepared s-g-C_3N_4@GQDs nanohybrids exhibit remarkably enhanced catalytic activity in ORR far better than the original s-g-C_3N_4 and GQDs, which is even comparable to those well-developed graphene-based materials. The s-g-C_3N_4@GQDs nanohybrids demonstrated in this study opens the way for constructing the new type of g-C_3N_4 based nanostructured materials not only for efficient catalytic in ORR process, but also for a large variety of electronic and photoelectronic device applications.

Acknowledgements

We thank the financial support from the 973 program of China (2011CB013000) and NSFC (21325415, 21174019, and 51161120361), Fok Ying Tong Education Foundation (no. 131043), and 111 Project 807012.

Notes and references

Key Laboratory of Cluster Science, Ministry of Education of China, Beijing Key Laboratory of Photoelectric/Electrophotonic Conversion Materials, School of Chemistry, Beijing Institute of Technology, Beijing 100081, P. R. China. E-mail: lqu@bit.edu.cn; zhaoyang-xiaolu@163.com

† Electronic Supplementary Information (ESI) available. See DOI: 10.1039/b000000x/

‡ These authors contributed equally to this work.

1 A. S. Arico, P. Bruce, B. Scrosati, J. M. Tarascon and W. V. Schalkwijk, *Nat. Mater*., 2005, **4**, 366–377.
2 Z. D. Wei, S. T. Zhang, Z. Y. Tang and H. T. Gou, *J. Appl. Electrochem*., 2000, **30**, 723–725.
3 A. Ermete, *Appl. Catal. B*., 2009, **88**, 1–24.
4 D. S. Geng, Y. Chen, Y. Chen, Y. L. Li, R. Li, X. Sun, S. Ye, S. Knights, *Energy Environ. Sci.*, 2011, **4**, 760–764.
5 K. P. Gong, F. Du, Z. H. Xia, M. Durstock, L. M. Dai, *Science*, 2009, **323**, 760–764.
6 J. Tian, A. Morozan, M. T. Sougrati, M. Lefèvre, R. Chenitz, J. P. Dodelet, D. Jones and F. Jaouen, *Angew. Chem.*, 2013, **125**, 7005–7008.
7 M. Lefevre, E. Proietti, F. Jaouen and J. P. Dodelet, *Science*, 2009, **324**, 71–74.
8 H. Gasteiger and N. Markovi, *Science*, 2009, **324**, 48–49.
9 D. S. Yu, E. Nagelli, F. Du, L. M. Dai, *J. Phys. Chem. Lett*., 2010, **1**, 2165–2173.
10 J. Zhang, K. Sasaki, E. Sutter and R. R. Adzic, *Science*, 2007, **315**, 220–222.
11 R. Bashyam and P. Zelenay, *Nature*, 2006, **443**, 63–65.
12 Y. Zheng, J. Liu, J. Liang, M. Jaroniec and S. Z. Qiao, *Energy Environ. Sci.*, 2012, ***5***, 6717–6731.
13 M. Groenewolt, M. Antonietti, *Adv. Mater.*, 2005, **17**, 1789−1792.
14 Y. Hou, Z. H. Wen, S. M. Cui, X. Guo, J. H. Chen, *Adv. Mater.*, 2013, **25**, 6291–6297.
15 J. Xu, Y. J. Wang and Y. F. Zhu, *Langmuir*, 2013, ***29***, 10566−10572
16 S. Yang, Y. Gong, J. Zhang, L. Zhan, L. Ma, Z. Fang, R. Vajtai, X. C. Wang and P. M. Ajayan, *Adv. Mater.*, 2013, ***25***, 2452–2456.

17 a) X. Zhang, X. Xie, H. Wang, J. Zhang, B. Pan and Y. Xie, *J. Am. Chem. Soc.*, 2013, **135** ,18–21; b) X. Wang, K. Maeda, A. Thomas, K. Takanabe, G. Xin, J. M. Carlsson, K. Domen and M. Antonietti, *Nat. Mater.*, 2009 , **8** , 76–80.
18 G. G. Zhang, M. W. Zhang, X. X. Ye, X. Q. Qiu, S. Lin, and X. C. Wang, *Adv. Mater.*, 2013, **26**, 805–809.
19 G. Liu, P. Niu, C. Sun, S. Smith, Z. Chen, G. Lu and H. Cheng, *J. Am. Chem. Soc.*, 2010, **13**, 11642–11648.
20 J. Hong, X. Xia, Y. Wang and R. Xu, *J. Mater. Chem.*, 2012, **22**, 15006–15012.
21 Z. Lin and X. Wang, *Angew. Chem. Int. Ed.*, 2013, **52**, 1735–1738.
22 Z. P. Zhang, J. Zhang, N. Chen and L. T. Qu, *Energy Environ Sci*., 2012, **5**, 8869–8890.
23 Y. Li, Y. Hu, Y. Zhao, G. Q. Shi, L. Deng, Y. B. Hou and L. T. Qu, *Adv Mater*, 2011, **23**, 776–780.
24 Y. Li, Y. Zhao, H. H. Cheng, Y. Hu, G. Q. Shi, L. M. Dai and L. T. Qu, *J. Am. Chem. Soc.*, 2012, **134**, 15–18.
25 J. K. Kim, M. J. Park, S. J. Kim, D. H. Wang, S. P. Cho and S. Bae, J. H. Park, and B. H. Hong, *ACS Nano*, 2013, **7**, 7207–7212.
26 J. H. Shen, Y. H. Zhu, X. L. Yang and C. Z. Li, *Chem. Commun.*, 2012, **48**, 3686–3699.
27 D. Y. Pan, J. C. Zhang, Z. Li and M. H. Wu, *Adv. Mater.*, 2010, **22**, 734–738.
28 H. X. Zhao, L. Q. Liu, Z. D. Liu, Y. Wang, X. J. Zhao and C. Z. Huang, *Chem. Commun.*, 2011, **47**, 2604–2606.
29 a) R. Liu, D, Wu, S, Liu, K. Koynov, W. Knoll and Q. Li, *Angew. Chem. Int. Ed.*, 2009, **48**, 4598–4601; b) L. Cao, S. Sahu, P. Anikumar, C. E. Bunker, J. Xu, K. A. S. Fernanodo, P. Wang, E. A. Guliants, K. N. Tackett and Y. P. Sun, *J. Am. Chem. Soc.*, 2011, **133**, 4754–4757; c) H. Li, X. He, Z. Kang, H. Huang, Y. Liu, J. Liu, S. Lian, C. H. A. Tsang, X. Yang and S. T. Lee, *Angew. Chem. Int. Ed.*, 2010, **49**, 4430–4434.
30 Y. Liu and P.Y. Wu, *ACS Appl Mater Interfaces*, 2013, **5**, 3362–3369.
31 L. X. Wang, C.G. Hu, Y. Zhao, Y. Hu, F. Zhao, N. Chen and L. T. Qu, *Carbon* , 2014, **74**, 170–179.
32 G. Q. He, Y. Song, K. Liu, A. Walter, S. Chen, S. W. Chen, *ACS Catal*, 2013, **3**, 831–838.
33 a) A. J. Bard and L. R. Faulkner, John Wiley & Sons, New York, 2001; b) W. Xiong, F. Du, Y. Liu, A. Perez, Jr., M. Supp, T. S. Ramakrishnan, L. Dai and L. Jiang, J. *Am. Chem. Soc.*, 2010, **132**, 15839–15841; c) S. Wang, D. Yu and L. Dai, *J. Am. Chem. Soc.*, **2011**, **133**, 5182–5185.
34 X. J. Bai, J. Li and C. B. Cao , *Materials Letters*, 2011, **65**,1101–1104.
35 F. Zhao, H. H. Cheng, Y. Hu, L. Song, Z. P. Zhang, L. Jiang, and L. T. Qu, *Sci. Rep.*, 2014, **4**, 5882–5888.
36 Y. Zheng, J. Liu, J. Liang, M. Jaroniec and S. Z. Qiao, *Energy Environ. Sci.*, 2012, **5**, 6717–6731.
37 Y. Q. Chang, F. Hong, C. X. He, Q. L. Zhang, and J. H. Liu, *Adv. Mater.*, 2013, **25**, 4794–4799.
38 Y.Zhao, C. Hu, L.Song, L. Wang, G. Shi, L. Dai and L. Qu, *Energy Environ. Sci.*,2014, **7**,1913–1918.
39 a)Y. Zhao, C. G. Hu, Y. Hu, H. H. Cheng, G. Q. Shi and L. T. Qu, *Angew. Chem. Int. Ed.*, 2012, **51**, 11371–11375; b) L. T. Qu, Y. Liu, J. B. Baek and L. M. Dai, *ACS Nano*, 2010, **4**, 1321–1326.
40 a) J. Liang, Y. Jiao, M. Jaroniec and S. Z. Qiao, *Angew. Chem. Int. Ed.* 2012, **51**, 11496–11500; b) J. Liang, X. Du, C. Gibson, X. W. Du and S. Z. Qiao, *Adv. Mater.*, 2013, **25**, 6226–6231.

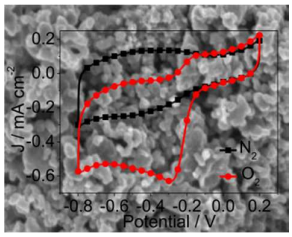

A rationally assembly of graphene quantum dots in-situ decorated onto the sulfur doped graphitic carbon nitride nanosheets for efficient electrocatalyst.